Journal of Physics and Chemistry of Solids 134 (2019) 209–213

Contents lists available at ScienceDirect

Journal of Physics and Chemistry of Solids

journal homepage: www.elsevier.com/locate/jpcs

Size effects on phonon response of bismuth nanoislands to ultrafast laser excitation

Hui Xiong[a], Ahmed Esmail[a,b], Hani E. Elsayed-Ali[a,b,*]

[a] Applied Research Center Old Dominion University, Newport News, VA, 23606, USA
[b] Department of Electrical and Computer Engineering, Old Dominion University, Norfolk, VA, 23529, USA

ARTICLE INFO

Keywords:
Bismuth nanoislands
Femtosecond laser excitation
Ultrafast electron diffraction

ABSTRACT

The lattice dynamics of bismuth nanoislands induced by ultrafast laser excitation is studied by ultrafast electron diffraction. The decay times of the Bragg peak intensity depend on the diffraction order. For 5-nm flat nanoislands, the decay time of the (110) diffraction order is close to the A_{1g} optical phonon decay time. When the thickness is increased to ~16 nm, the excitation energy is dissipated into low energy phonons, making energy transport diffusive, thus leading to a longer decay time. The temporal evolution of the (012) Bragg diffraction peak shows a two exponential decay with a second decay time of ~40 ps emerging when the nanoislands are 5 nm thick and the laser fluence is lower than 1.5 mJ/cm^2. This second decay may be attributed to a phonon bottleneck caused by size restriction.

1. Introduction

Ultrafast pump-probe studies using optical/near infrared, x-ray, and electron pulses have enabled the studies of the transient structural evolution upon excitation by femtosecond laser pulses with a time resolution up to tens of femtoseconds [1–8]. Most studies on the transient structural evolution were carried out on thin films [4,9–12] and crystalline surfaces [3,13,14]. In the past few years, such studies have been extended to probe size-confined systems, such as nanoparticles [7,8,15,16], flat nanoislands [17], and nanowires [18] with the aim of revealing size-dependent electronic and structural mechanisms [19]. For example, a transient lattice contraction due to hot electron blast force was observed over several picoseconds in Bi nanoparticles [16], and the decay time of the transient electron diffraction of GaAs nanoparticles was found to be size-dependent [15]. Among those size-dependent phenomena, the phonon bottleneck effect is expected to be universal because the phonon energy levels become discrete in size-confined materials, leading to insufficient relaxation via phonon interactions [19]. Yet, only a few experimental studies on the effects of the phonon bottleneck have been reported [20,21]. Many open questions remain on the roles of the electrons, holes, and phonons in the ultrafast response of size-confined materials.

Among the studied materials, crystalline Bi receives great interests because of its semimetallic nature and pronounced structural response to laser excitation [2,3,6,7,16,17,22,23]. Numerous phenomena have been studied in Bi, such as sub-picosecond disordering [24–26], laser-driven phase transition [27,28], and squeezed phonon states [1,4]. Theoretical explanations of the relaxation dynamics in Bi crystals excited by ultrafast lasers usually employ the longitudinal A_{1g} phonons as an intermediate energy transporter [2,3]. Particularly, displacive excitation of coherent phonons is widely used to describe optical reflectivity oscillations induced by the fully-symmetric A_{1g} phonons in Bi after absorption of energy from the femtosecond laser pulse [29,30]. Upon femtosecond photo-excitation, the density of excited carriers in the conduction band is increased through the inter-band transition, and the electron gas temperature is raised through photon absorption. The impact of these effects is to displace the equilibrium atomic positions due to the change in the atomic bond strength, which eventually launches large amplitude coherent oscillations corresponding to the A_{1g} phonons [3]. The generation of the A_{1g} phonons occurs in ~100 fs, which is much shorter than the temporal resolution in the present ultrafast electron diffraction (UED) experiment and is not a major factor in the present work [2,3]. Damping of the A_{1g} phonons starts by nonlinear phonon-phonon interactions dephasing the harmonic vibrations which lead to the onset of thermal expansion [3]. Decay of the A_{1g} phonons into two acoustic phonons has been suggested to be the dominant underlying mechanism that contributes to a lattice thermalization time in about 5–20 ps [3]. The decay time of the A_{1g} phonons in Bi is well characterized by pump-probe reflectivity measurement, because it is observed in the reflectivity oscillation resulting from electron

* Corresponding author. Applied Research Center Old Dominion University, Newport News, VA, 23606, USA.
E-mail address: helsayed@odu.edu (H.E. Elsayed-Ali).

https://doi.org/10.1016/j.jpcs.2019.06.014
Received 20 May 2019; Received in revised form 7 June 2019; Accepted 13 June 2019
Available online 14 June 2019
0022-3697/

density oscillation induced by the A_{1g} phonons [3,6].

In the present UED study, electron pulses are used to obtain transmission diffraction patterns of the Bi nanoislands. The lattice structural evolution detected by changes in the Bragg diffraction peaks is studied. The intensities of the Bragg diffraction peaks depend on the mean-square displacement of the atoms. Assuming harmonic oscillation of the atoms, the decay of peak intensity in UED follows the Debye-Waller treatment [31,32], where the intensity of the diffraction peaks is reduced due to the vibration of atoms around its equilibrium position. This is considered a measure of the lattice temperature; however, extension of this treatment to define a temperature is not strictly valid if the phonon distribution has not reached equilibrium. In transmission UED, the absorbed pump laser energy is not uniformly deposited in the sample as it decreases with sample depth. The absorption skin depth of Bi at 800 nm is ~14 nm, smaller than the thickness of most samples studied by transmission UED; hence ballistic and diffusive heat transport may not be negligible. It was previously shown that, when the size of a GaAs nanoparticle is smaller than the inelastic phonon mean-free path, slower acoustic phonon-phonon scattering is prevented, and the energy is localized in high-energy acoustic modes that "travel" coherently within the film, resulting a decay time of Bragg diffraction peaks that is close to the decay time of the longitudinal optical phonons in GaAs [15]. As the size of the GaAs nanoparticle increases, slower phonon-phonon scattering within the acoustic population takes place, and the lattice thermalization becomes diffusive in nature [15]. In that case, a much longer Bragg diffraction peak decay time is observed [7,10]. The inelastic phonon mean-free path is thus the decisive parameter that determines the decay time of the Bragg diffraction peaks.

To clarify the relation between the A_{1g} phonon decay and the transient UED peak intensity decay in Bi, we measured the transient decay time for UED diffraction peaks from flat nanoislands as functions of laser fluence and sample temperature. When the sample is 5 nm thick and the laser fluence is $< 1.5\,mJ/cm^2$, the decay time of (012) Bragg diffraction peak has a two exponential structure with the second decay time of ~40 ps. This second decay time may be attributed to phonon bottleneck effect due by size limitation.

2. Experiment

The experimental setup is described elsewhere [7,10,16,17]. Briefly, an electron pulse is generated by photoemission from a silver thin-film photocathode excited by UV pulse at 267 nm generated by frequency tripling of 110 fs duration, 1 kHz, 800 nm fundamental laser with two cascaded (barium borate) BBO crystals. The photocathode is connected to a high voltage supply, which is set at negative 35 kV. The electrons are accelerated towards a grounded metal anode with a pinhole of 150 μm in the center. After passing through the pinhole, the electrons are collimated and directed toward the sample by a set of electromagnets located outside the vacuum. The electron probe pulse is used in the transmission diffraction geometry. The diffraction pattern is formed on micro-channel plate (MCP)-phosphorus screen assembly, and captured by CCD camera PIXIS-1024. The samples are mounted on a resistive heating stage and exposed to the 800 nm pump laser pulse with variable fluence controlled by a laser attenuator consisting of a half-waveplate and a thin film polarizer. The time delay between the electron and laser pulses was controlled by an optical translation stage. The temporal resolution of the UED setup is ~1.5 ps at this photocathode voltage and photocathode excitation.

3. Results and discussion

Bismuth film of 5 nm average thickness was grown by thermal evaporation on 3 mm diameter copper transmission electron microscopy (TEM) grids coated with < 10 nm thick carbon layers. As shown in the TEM image in Fig. 1(a), the film is not continuous. The Bi flat islands are formed after annealing with the fundamental wavelength of the femtosecond laser pulses at a fluence of $\sim 2.4\,mJ/cm^2$ operating at 1 kHz repetition rate (Fig. 1(b)), the annealing process takes about 2 h. If the sample was heated at 450 K when it is being annealed by the laser, the Bi islands melt, resulting in its quenching to form Bi nanoparticles (Fig. 1(b)). Fig. 1 also shows the corresponding electron diffraction patterns obtained in a transmission electron microscope. Due to the shape irregularity, the mean size of the nanoislands is less relevant, hence we estimate the average crystal size in the islands to be ~7.2 nm by the Scherrer equation using the full-width at half-maximum of the (110) peak. On the other hand, the size of the nanoparticles was obtained by TEM images, and the mean length of the major axis and the minor axis of the nanoparticles were 16 ± 4 and 14 ± 4 nm, respectively.

Fig. 2 shows the normalized time-resolved intensity of the (012) and (110) Bragg diffraction peaks for pump laser fluence of 1.5 and 2.5 mJ/cm^2. The behavior of the diffraction intensity for the (012) diffraction peak was fitted to a double exponential decay function:

$$\frac{I}{I_0} = \begin{cases} 1 & t \le 0 \\ A + B \times e^{-t/\tau_1} + C \times e^{-t/\tau_2} & t > 0 \end{cases} \quad (1)$$

The fitting parameters are summarized in Table 1. Fitting parameters obtained at a laser fluence of $3.3\,mJ/cm^2$ are also shown in Table 1. The damping of the normalized intensity depends on the laser fluence and the diffraction peak order. The second exponential decay was observed only for laser fluence at $1.5\,mJ/cm^2$ on the (012) diffraction order. The diffraction peak intensity is reduced with heating due to the increased vibration of atoms around their equilibrium positions. Thus, the two exponential decays with decay times depicted as τ_1 and τ_2, can be treated as two different energy coupling dynamics leading to lattice heating.

The slower decay time τ_2 ~37 ps on the (012) Bragg peak was only observed on nanoislands at a laser fluence at $1.5\,mJ/cm^2$. Coherent acoustic phonons have a decay time of tens of ps in Bi thin films [10,12], but if the observed ~37 ps day is connected with the decay of coherent acoustic phonons, the Bragg diffraction peak intensity would show some oscillation, which is not observed in the present experiment. A plausible explanation of the presence of a second decay time is that a phonon bottleneck effect, induced by the size confinement, slows down the thermal relaxation process. The energy levels in a size-confined material are discrete and thermal relaxation becomes inefficient due to the lack of efficient cascade momentum relaxation within a continuum energy band that is available in non-confined materials. The temperature rise rate for the nanoislands due to ultrafast excitation according to Debye-Waller treatment [13,14] was found to be $64\,K\,mJ^{-1}\,cm^2$. High laser fluence, for example, $3.3\,mJ/cm^2$ in our experiment, would bring the temperature of nanoislands to ~511 K, only ~35 K lower than the melting point of bulk bismuth. At this temperature, phenomena such as lattice instability, and surface melting, broadens the discrete energy levels caused by size confinement. Therefore, the thermal relaxation processes become more efficient, and the time-dependent Bragg peak intensity at the high laser fluence does not show the slower decay component. This could be a reason that a phonon bottleneck effect is not observed in the UED experiment.

The faster decay τ_1 is related to the normal lattice heating processes we described above. Clearly, the decay time τ_1 is longer for the (012) diffraction order than for the (110), indicating an anisotropic lattice response. Anisotropic thermal response upon ultrafast laser excitation has been observed in Bi nanoparticles [7,16], flat nanoislands [17], and polycrystalline film [10]. This anisotropy shows that the energy transfer from the excited carriers and coherent phonons to the lattice is anisotropic. The anisotropic Debye-Waller factor e^{-W} is given by Refs. [31,32].

$$W = \beta_{11}(h^2 + hk + k^2) + \beta_{33}l^2 \quad (2)$$

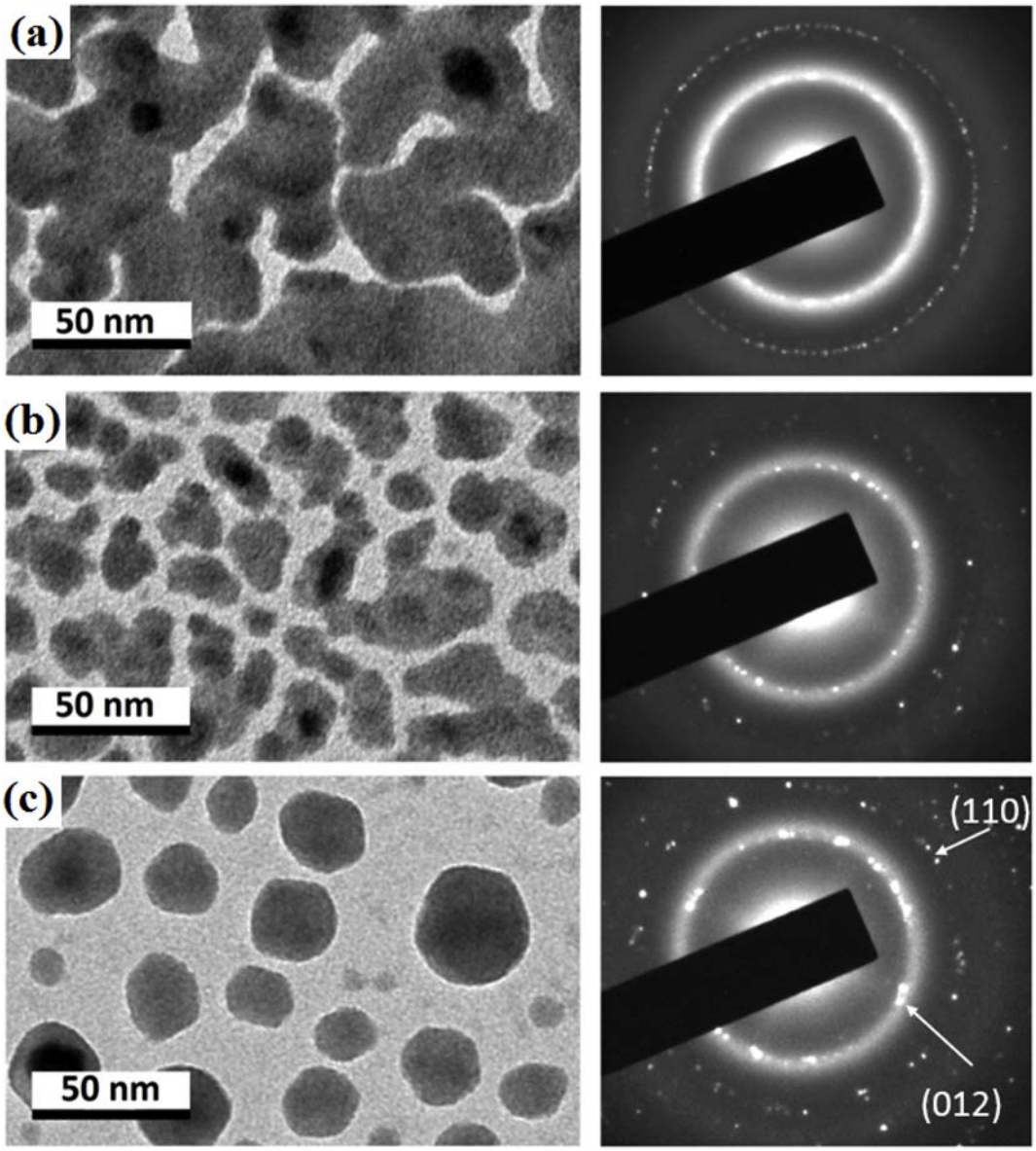

Fig. 1. TEM and diffraction patterns of Bi: (a) the as-deposited 5-nm Bi film, (b) femtosecond laser annealed nanoislands, and (c) simultaneously annealed thermally and with femtosecond laser pulses resulting in formation of nanoparticles. The ring overlaps on the (012) diffraction peaks is due to the disordered state from the surface, which can be found in almost all Bi nanoparticles synthesized by chemical methods [23,33]. The mean length of the major axis and the minor axis of the nanoparticles were 16 and 14 nm.

$$B_{\parallel} = \frac{4\beta_{33}}{c^{*2}} = 8\pi^2 U_{\parallel}^2 \tag{3}$$

$$B_{\perp} = \frac{4\beta_{11}}{a^{*2}} = 8\pi^2 U_{\perp}^2 \tag{4}$$

where β_{ij} is anisotropic temperature factor; $U_{\parallel}^2$ and $U_{\perp}^2$ denote mean-square displacement of the atoms parallel and perpendicular to the hexagonal *c-axis*, respectively; *h*, *k*, and *l* are Rhombohedral Miller indices, a^* and c^* are the axis lengths. In the present work, the electron diffraction from the (012) and (110) planes are investigated. Therefore, the decay terms of the two diffraction peak intensities in the Debye-Waller factor are

$$W_{012} = 2\pi^2 a^{*2} U_{\perp}^2 + 8\pi^2 c^{*2} U_{\parallel}^2 \tag{5}$$

$$W_{110} = 6\pi^2 a^{*2} U_{\perp}^2 \tag{6}$$

An important inference from these Debye-Waller factors is that the decay of the (110) Bragg diffraction peak intensity is only determined by the vibration perpendicular to the *c-axis*, while the decay of the (012) peak intensity is related to vibration perpendicular and parallel to the *c-axis*. Upon the femtosecond excitation, coherent A_{1g} phonons along the *c-axis* are induced. The dominant decay pathway for the A_{1g} phonons is the decay into two high-energy acoustic phonons, increasing the mean-square atomic displacement $U_{\perp}^2$, with $U_{\perp}^2$ increasing at the same time scale as the decay of the A_{1g} phonons. In case of thin sample, like the 5-nm nanoisland used in this experiment, the high-energy phonons originating from the decay of the A_{1g} phonons, distribute their energy evenly inside the sample. In this scenario, where thermal transport is negligible, the decay of the (110) Bragg peak will depend on the decay time of the A_{1g} phonons. To the contrary, if the sample is thicker than the mean-free path of the high-energy acoustic phonons, the high-energy acoustic phonons generated from the decay of the A_{1g} phonons would do not distribute their energy evenly inside the sample. Slower phonon-phonon scattering within the acoustic population takes place, and thermal transport leads to a longer time to reach thermal equilibrium throughout the nanoparticle.

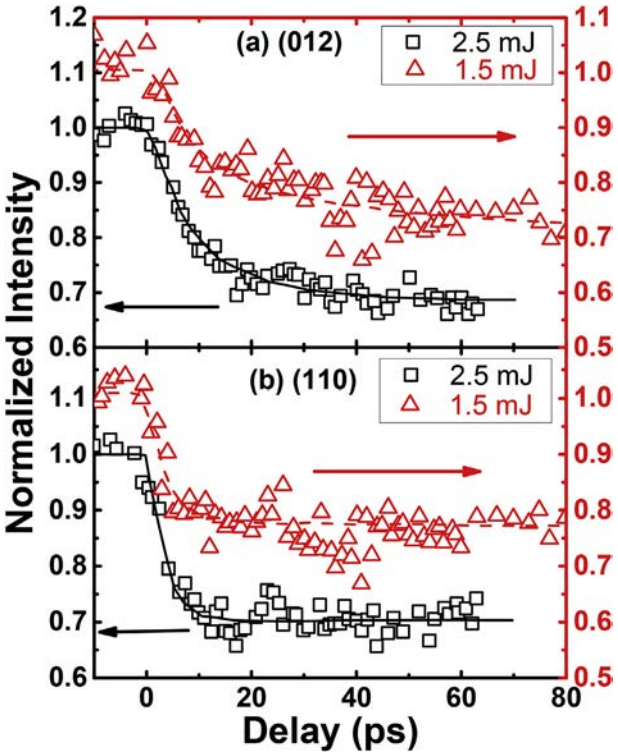

Fig. 2. Time dependent normalized Bragg diffraction peak intensity for (a) (012), and (b) (110) diffraction orders of 5-nm-thick Bi nanoislands at pump laser fluence of 1.5 and 2.5 mJ/cm^2. Data sets at 2.5 mJ/cm^2 were lowered 0.1 for visibility.

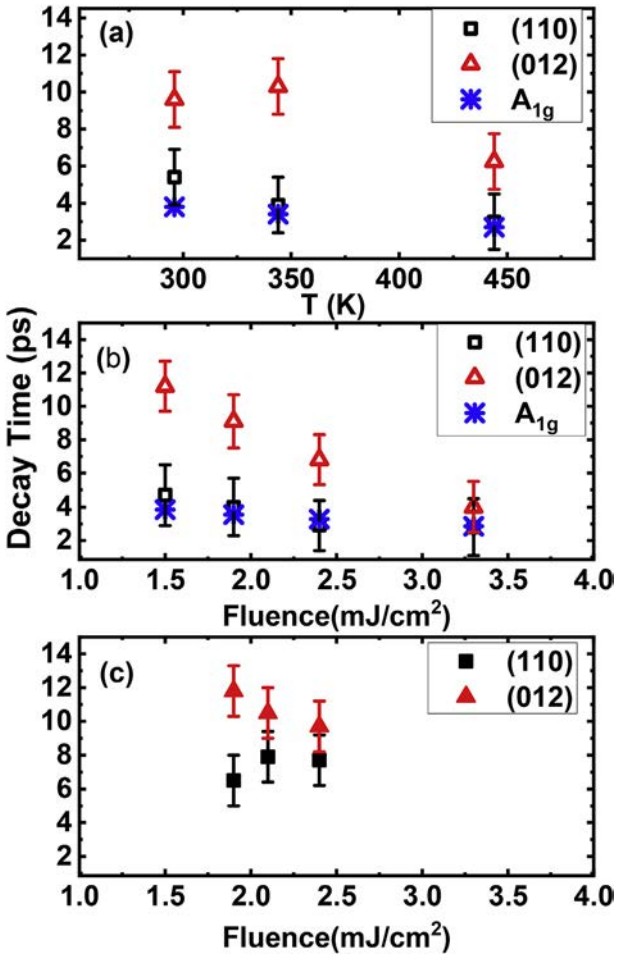

Fig. 3. The decay time of Bragg peak intensity for the (012) and (110) planes of 5-nm-thick Bi nanoislands at different temperatures for pump laser fluence 2.5 mJ/cm^2, and (b) for different pump laser fluence at room temperature. The blue-star are damping time for A_{1g} phonons on bulk bismuth surface, extrapolated from Ref. [3]. (c) The decay time for Bragg peak intensity for the (012) and (110) diffraction orders of Bi nanoparticles. The mean length of the major axis and the minor axis of the nanoparticles were 16 and 14 nm.

To further identify the origin of the size-dependent decay time of the Bragg diffraction orders, we obtained the decay time of the Bragg peak intensity of the (012) and (110) diffraction orders at different base temperatures and for different laser fluence by systematically measuring the time dependent diffraction order intensity change of the (012) and (110) Bragg diffraction orders. The results are shown in Fig. 3 (a) and (b). The decay times for Bragg peaks from (012) and (110) diffraction orders are reduced with the increased laser fluence and base temperature.

Because the diffraction peak intensity change is related to the mean-square amplitude of the phonons involved, the temporal evolution of the coherent A_{1g} phonons is closely related to the decay time of the Bragg peaks. Here, we extrapolate the damping time of the A_{1g} phonons on Bi bulk surface from Ref. [3], and plot it in Fig. 3. The damping time of the A_{1g} phonons matches well the decay time of the (110) Bragg peak. Apparently, the decay of the (110) Bragg peak intensity of flat nanoislands is dominated by damping of A_{1g} phonons. It is known that the A_{1g} phonons vibrate parallel to the (110) plane and the *c-axis*. Thus, the amplitude of the A_{1g} phonons is not reflected on the Bragg peak intensity. The measured decay time of the (110) Bragg peak intensity is essentially linked to the speed of energy transfer to phonons vibrating perpendicular to the *c-axis*. For a nanoislands, which restricts one dimension to a smaller value than the inelastic phonon mean-free path, the Bragg peak intensity decay time becomes close to the damping time of the longitudinal optical phonons. In bismuth, 80% of thermal conductivity at room temperature is contributed by phonons with mean-free path < 15 nm [34], which is larger than the ~5 nm thickness of the nanoislands. Thus, the observed decay time for (110) diffraction peak is close to the A_{1g} damping time. Several fast processes that occur right after carrier excitation, such as electron-hole recombination [35] and squeezed phonon state [1,4] are not discussed here. These processes occur at the beginning of the relaxation processes, thus are not affecting the observed decay time.

As for the (012) Bragg peak, Eq. (5) indicates that the decay of this

Table 1
The summary of fitting parameters.

peak	Intensity (mJ/cm^2)	A	B	τ_1 (ps)	C	τ_2 (ps)	Reduced Chi-squared
(012)	1.5	0.71 ± 0.02	0.25 ± 0.05	5.0 ± 2.3	0.16 ± 0.04	37 ± 22	7.1×10^{-4}
	2.5	0.69 ± 0.00	0.25 ± 0.01	9.1 ± 1.6	–	–	3.6×10^{-4}
	3.3	0.45 ± 0.00	0.59 ± 0.02	4.0 ± 1.5	–	–	4.4×10^{-4}
(110)	1.5	0.75 ± 0.00	0.22 ± 0.01	4.7 ± 1.8	–	–	9.8×10^{-4}
	2.5	0.70 ± 0.00	0.28 ± 0.02	4.0 ± 1.7	–	–	5.6×10^{-4}
	3.3	0.42 ± 0.00	0.51 ± 0.03	2.8 ± 1.7	–	–	7.6×10^{-4}

peak depends on both the mean-square displacements perpendicular and parallel to *c-axis*. The A_{1g} phonons are excited on 100 fs time scale due to the fast electron-phonon interaction. However, the fast increase in $U_{\parallel}^2$ associated with the A_{1g} phonons is not observed in the present experiment due to the limited temporal resolution of our UED setup. The decay of the A_{1g} phonons quickly raises $U_{\perp}^2$, which lead to the quick decay of the (110) peak. A_{1g} phonons predominantly decay into two high energy acoustic phonons. Equilibrium is reached after the phonons are dephased and energy is evenly redistributed in all degrees of freedom. However, the phonons with vibration components along the *c-axis* reach equilibrium slower due to the energy reserved in the decaying coherent A_{1g} phonons along the *c-axis* slows energy backflow. Therefore, the equilibrium on *c-axis* is reached later, leading to a slower decay of the (012) Bragg peak.

If the temperature of the sample is increased, the single phonon damping rate would increase with the square of the temperature [3]. Thus, the damping time of the A_{1g} phonons decreases with temperature causing the shorter decay time observed in the UED experiment. Increasing the laser fluence also leads to a higher temperature, hence decreases the decay time. We note that the thickness of the nanoislands and nanoparticles is critical in the observed decay time change. As shown in Fig. 3(c), for the ~16 nm Bi nanoparticles, the decay times of the (012) and (110) diffraction orders are much longer than the damping time of the A_{1g} phonons. Here, although the ~16 nm Bi is comparable with the mean-free path of the phonons, the larger side of the size distribution contribute to the observed extended decay time.

4. Conclusion

We studied the ultrafast lattice thermal response of 5-nm flat nanoislands and 16-nm nanoparticles by UED. The size of the nano-material plays an important role in their thermal response to laser excitation. For the 5-nm thick flat nanoislands, the decay time of the (110) Bragg diffraction peak from (110) planes was found to be close to the A_{1g} damping time, and was attributed to the reduced effect of the slower acoustic phonon-phonon scattering due to the nanoisland thickness being smaller than the mean-free path of the acoustic phonons. A second exponential decay time of ~40 ps emerged for the (012) Bragg diffraction peak, which is observed when the nanoislands are 5 nm and laser fluence is lower than 1.5 mJ/cm^2. This longer decay time may be attributed to a phonon bottleneck effect caused by size restriction.

Acknowledgement

This study is based on research supported by the National Science Foundation under Grant No. 1708717.

References

[1] S.L. Johnson, P. Beaud, E. Vorobeva, C.J. Milne, É.D. Murray, S. Fahy, G. Ingold, Phys. Rev. Lett. 102 (2009) 175503.
[2] D. Boschetto, E.G. Gamaly, A.V. Rode, B. Luther-Davies, D. Glijer, T. Garl, O. Albert, A. Rousse, J. Etchepare, Phys. Rev. Lett. 100 (2008) 027404.
[3] T. Garl, E.G. Gamaly, D. Boschetto, A.V. Rode, B. Luther-Davies, A. Rousse, Phys. Rev. B 78 (2008) 134302.
[4] K. Sokolowski-Tinten, R.K. Li, A.H. Reid, S.P. Weathersby, F. Quirin, T. Chase, R. Coffee, J. Corbett, A. Fry, N. Hartmann, et al., New J. Phys. 17 (2015) 113047.
[5] S. Nie, X. Wang, H. Park, R. Clinite, J. Cao, Phys. Rev. Lett. 96 (2006) 025901.
[6] A.A. Melnikov, O.V. Misochko, S.V. Chekalin, J. Appl. Phys. 114 (2013) 033502.
[7] A.R. Esmail, A. Bugayev, H.E. Elsayed-Ali, J. Phys. Chem. C 117 (2013) 9035.
[8] X. Wang, H. Rahmani, J. Zhou, M. Gorfien, J.M. Plaskus, D. Li, R. Voss, C.A. Nelson, K.W. Lei, A. Wolcott, et al., Appl. Phys. Lett. 109 (2016) 153105.
[9] A. Bugayev, H.E. Elsayed-Ali, J. Phys. Chem. Solids 129 (2019) 312.
[10] A. Bugayev, A. Esmail, M. Abdel-Fattah, H.E. Elsayed-Ali, AIP Adv. 1 (2011) 012117.
[11] M.H. Abdel-Fattah, A. Bugayev, H.E. Elsayed-Ali, Phys. B Condens. Matter 492 (2016) 65.
[12] T. Shin, Thin Solid Films 666 (2018) 108.
[13] E.A. Murphy, H.E. Elsayed-Ali, J.W. Herman, Phys. Rev. B 48 (1993) 4921.
[14] J.W. Herman, H.E. Elsayed-Ali, Phys. Rev. Lett. 69 (1992) 1228.
[15] G.M. Vanacore, J. Hu, W. Liang, S. Bietti, S. Sanguinetti, A.H. Zewail, Nano Lett. 14 (2014) 6148.
[16] A. Esmail, M. Abdel-Fattah, H.E. Elsayed-Ali, J. Appl. Phys. 109 (2011) 084317.
[17] A.R. Esmail, H.E. Elsayed-Ali, Appl. Phys. Lett. 99 (2011) 161905.
[18] M.C. Newton, M. Sao, Y. Fujisawa, R. Onitsuka, T. Kawaguchi, K. Tokuda, T. Sato, T. Togashi, M. Yabashi, T. Ishikawa, et al., Nano Lett. 14 (2014) 2413.
[19] F.W. Wise, Acc. Chem. Res. 33 (2000) 773.
[20] Y.Q. Huang, I.A. Buyanova, X.J. Yang, A. Murayama, W.M. Chen, Phys. Rev. Appl. 9 (2018) 044037.
[21] J.J.H.A. van Hest, G.A. Blab, H.C. Gerritsen, C. de Mello Donega, A. Meijerink, J. Phys. Chem. C 122 (2018) 3985.
[22] E.F. Cave, L.V. Holroyd, J. Appl. Phys. 31 (1960) 1357.
[23] Q. Li, H. Zhu, L. Zheng, L. Fan, Y. Ren, J. Chen, J. Deng, X. Xing, Adv. Sci. 3 (2016) 1600108.
[24] J.J. Li, J. Chen, D.A. Reis, S. Fahy, R. Merlin, Phys. Rev. Lett. 110 (2013) 047401.
[25] B. Arnaud, Y. Giret, Phys. Rev. Lett. 110 (2013) 016405.
[26] M. Hase, M. Kitajima, S.-i. Nakashima, K. Mizoguchi, Phys. Rev. Lett. 88 (2002) 067401.
[27] G. Sciaini, M. Harb, S.G. Kruglik, T. Payer, C.T. Hebeisen, F.-J.M. z. Heringdorf, M. Yamaguchi, M. H.-v. Hoegen, R. Ernstorfer, R.J.D. Miller, Nature 458 (2009) 56.
[28] K. Sokolowski-Tinten, C. Blome, J. Blums, A. Cavalleri, C. Dietrich, A. Tarasevitch, I. Uschmann, E. Förster, M. Kammler, M. Horn-von-Hoegen, et al., Nature 422 (2003) 287.
[29] H.J. Zeiger, J. Vidal, T.K. Cheng, E.P. Ippen, G. Dresselhaus, M.S. Dresselhaus, Phys. Rev. B 45 (1992) 768.
[30] T.K. Cheng, J. Vidal, H.J. Zeiger, G. Dresselhaus, M.S. Dresselhaus, E.P. Ippen, Appl. Phys. Lett. 59 (1991) 1923.
[31] R.M. Goodman, H.H. Farrell, G.A. Somorjai, J. Chem. Phys. 48 (1968) 1046.
[32] P. Fischer, I. Sosnowska, M. Szymanski, J. Phys. Condens. Matter 11 (1978) 1043.
[33] H. Yu, P.C. Gibbons, K.F. Kelton, W.E. Buhro, J. Am. Chem. Soc. 123 (2001) 9198.
[34] S. Lee, K. Esfarjani, J. Mendoza, M.S. Dresselhaus, G. Chen, Phys. Rev. B 89 (2014) 085206.
[35] J. Cho, T.Y. Hwang, A.H. Zewail, Proc. Natl. Acad. Sci. U.S.A. 111 (2014) 2094.